

## Evidence for Jet Collimation in SS 433 with the Chandra HETGS

Masaaki Namiki<sup>1</sup>\*, Nobuyuki Kawai<sup>2</sup>, Taro Kotani<sup>2</sup> and Kazuo Makishima<sup>3,4</sup>

<sup>1</sup> Earth and Space Science, Graduate School of Science, Osaka University, 1-1  
Machikaneyama, Toyonaka, Osaka, Japan

<sup>2</sup> Department of Physics, Faculty of Science, Tokyo Institute of Technology, 2-12-1,  
Oookayama, Meguro, Tokyo, Japan

<sup>3</sup> Department of Physics, University of Tokyo, 7-3-1, Hongo, Bunkyo, Tokyo, Japan

<sup>4</sup> The Institute of Physical and Chemical Research, 2-1, Hirosawa, Wako, Saitama, Japan

**Abstract** High-resolution X-ray spectra of SS 433 obtained at an anti-eclipse, during an eclipse, and after a binary egress with the Chandra High Energy Transmission Grating Spectrometer (HETGS) were studied. Many Doppler-shifted X-ray emission lines from highly ionized elements were detected. All of the Doppler-shifted emission lines are found to be broader than the instrumented resolution. Neither the measured line widths nor their dependence on the atomic number can be explained by thermal broadening alone. Alternative explanations of the observed line widths are discussed, including in particular a progressive jet collimation along its axis.

**Key words:** Jets — Stars: individual (SS 433) — Stars: binaries: general — X-rays: individual (SS 433) — X-rays: spectra

### 1 INTRODUCTION

SS 433 is an enigmatic X-ray binary (orbital period  $\sim 13.1$  d) with a bipolar jet ejecting matter at a relativistic velocity of  $0.26c$ . The jet axis precesses with a period of  $\sim 162.5$  d. Although SS 433 has been studied for more than 20 years since its discovery, its fundamental properties and the nature of the compact object remain unknown.

The Chandra High Energy Transmission Grating Spectrometer (HETGS) is ideal for an attempt to significantly improve our knowledge obtained with previous missions. Marshall et al. (2002) reported on the first observation of SS 433 using the HETGS. The lines were measurably broadened and the widths did not depend significantly on the line-center energy, suggesting that the emission occurs in a freely expanding region of constant collimation with an opening angle of  $1^\circ.26$ . While, Namiki et al. (2003) reported on another HETGS observation, and found a dependence of the line widths on the atomic number. They concluded that its dependence was successfully explained by assuming the line widths originate from the jet opening angle, and that the angle becomes narrower as the jets travel away from the central engine. There are some inconsistency between these two reports, though the same instruments were used. In this

---

\* E-mail: [namiki@ess.sci.osaka-u.ac.jp](mailto:namiki@ess.sci.osaka-u.ac.jp)

paper, three datasets of HETGS observation, including the above both data, are treated in the same way and interpreted in an uniform picture of the jets in the SS 433 system.

## 2 OBSERVATIONS

The present observations of SS 433 were performed with the Chandra HETGS on 1999 September 23, 2001 March 16, and 2001 May 12. The corresponding orbital phases were 0.658, 0.965, and 0.283 (Gladyshev et al. 1987), respectively. Usually, the jet directed to the east (called “blue jet”) is approaching us, and that to the west (“red jet”) is receding. However, on 2001 May 12, SS 433 was in the reversal precessional phase, in such a way that the blue jet is receding and the red one is approaching. This reversal occurs for a minor fraction ( $\sim 50$  d) of the 162 d precession period.

The observation log is shown in Table 1. All the data were acquired in the ACIS-S timed exposure mode, and processed in a standard way. The average flux of SS 433 in the 1–10 keV band was 13.5, 13.3, and  $8.7 \times 10^{-11}$  erg s $^{-1}$  cm $^{-2}$  for the observation ID-0106, -1019, and -1942, respectively. These are typical values of SS 433 at each precessional and binary phase.

**Table 1** Observation Log

Observation ID	Start time (UT)	End time (UT)	Orbital phase*	Exposure time
0106	1999/09/23 12:20	1999/09/23 21:14	$0.658 \pm 0.014$	28.6 ks
1019	2001/03/16 22:21	2001/03/17 05:28	$0.965 \pm 0.011$	25.7 ks
1942	2001/05/12 10:38	2001/05/12 16:33	$0.283 \pm 0.009$	19.7 ks

\* Calculated from the parameters given by Gladyshev et al. (1987).

## 3 ANALYSIS AND RESULTS

### 3.1 Data reduction

The data of three observations were treated and processed in the same way. The spectral extraction and data reduction were all performed with the standard pipeline for the Chandra HETGS. The fits are evaluated via minimum likelihood method, the energy-bin widths are chosen to be comparable to the energy resolution of the data. This method was applied in the same way as Namiki et al. (2003), and was fully described in that paper. The detailed spectral analysis of ID-0106 have been presented in Marshall et al. (2002), and those of ID-1019 and -1942 are in Namiki et al. (2003) and Namiki (2003). Since these three observations are very similar to each other, the analysis of ID-1942 of them is mainly presented in this paper.

### 3.2 Spectral analysis of ID-1942

#### 3.2.1 hard energy band spectra

In figure 1, the HEG/HETGS spectrum in 5.5–8.5 keV energy band around the iron K lines is fitted with a model consisting of a power-law continuum and broad Gaussian lines (Marshall et al. 2002; Namiki et al. 2003; Namiki 2003). The Gaussians for the stationary fluorescent lines ( $z = 0$ ) were kept narrow, because they are thought to come from a vicinity of the compact object. The fitting model is given, as a function of energy  $E$ , as:

$$\begin{aligned}
 e^{-\sigma(E)N_{\text{H}}} \times & \left[ A \times E^{-\Gamma} + \text{Fe I K}\alpha_{z=0} + \text{Fe I K}\beta_{z=0} \right. \\
 & + (\text{Fe XXV K}\alpha + \text{Fe XXVI K}\alpha + \text{Ni XXVII K}\alpha + \text{Fe XXV K}\beta)_{z=z_{\text{red}}} \\
 & \left. + (\text{Fe XXV K}\alpha + \text{Fe XXVI K}\alpha + \text{Ni XXVII K}\alpha + \text{Fe XXV K}\beta)_{z=z_{\text{blue}}} \right], \quad (1)
 \end{aligned}$$

where  $\sigma(E)$  is the photo-electric cross-section at  $E$ ,  $N_{\text{H}}$  is the equivalent hydrogen column density (determined in the lower energy band; see § 3.2.2), while  $A$  and  $\Gamma$  are the normalization and photon index of the power-law continuum, respectively.

The fitting model includes Gaussian components corresponding to ten emission lines, as specified by the line names in equation (1). The rest-frame center energies of the lines were fixed to the theoretical values, while the overall Doppler shifts of the blue and red jets were set free; the redshift is common among all of the lines belonging to the same jet. The obtained width of the lines has been constrained as  $\sigma \sim 44.5^{+12.9}_{-7.3}$  eV, or  $2100^{+600}_{-340}$  km s<sup>-1</sup> in terms of the velocity dispersion. It has been confirmed that these broadenings of the lines are not due to the precession movement of the SS 433 system during total data span, nor to the triplet structures of helium-like ions (Namiki et al. 2003).

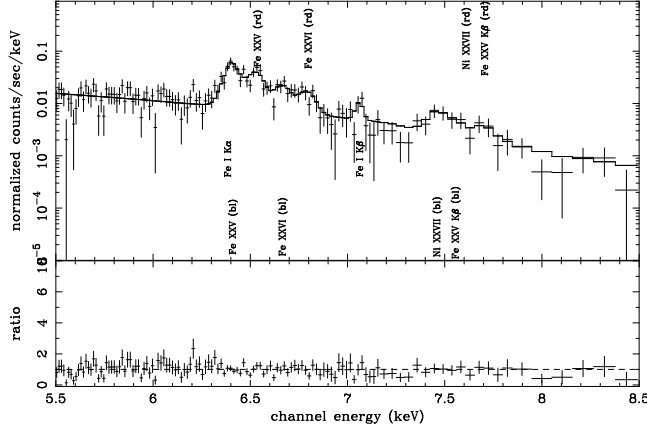


**Fig. 1** Chandra HETGS spectrum of SS 433 (ID-1942) around iron K-line energy band. The solid histograms represent the best-fit model. The location of lines are labeled with ion species and the jet identification; “bl” and “rd” denote lines from the blue and red jet, respectively. The bottom panel shows the intensity ratio against the best-fit model.

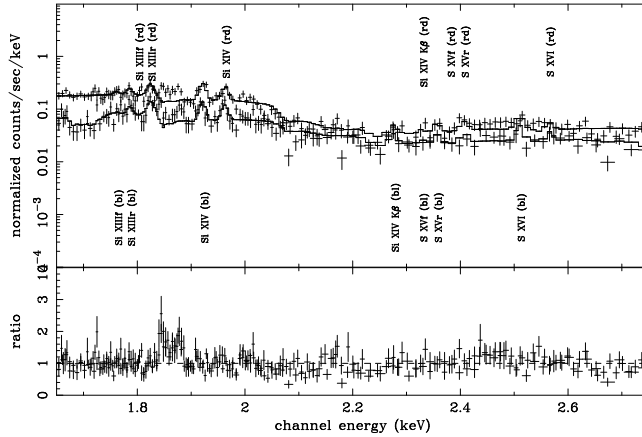


**Fig. 2** Chandra HEG (lower) and MEG (upper) spectra of SS 433 (ID-1942), shown over the silicon K-line energy band. The subscripts “r” and “f” are for the resonance and forbidden components, respectively. The other annotations are the same as that of Fig. 1.

### 3.2.2 soft energy band spectra

Figure 2 shows the spectra obtained by the MEG and HEG in the soft band (1.5 – 4.0 keV). Below, they are fitted jointly. First, the data were fitted with a model of a power-law continuum and broad Gaussian lines with photoelectric absorption, just in the same way as was performed in § 3.2.1, using the redshifts derived there as initial values. The fitting model is given as:

$$e^{-\sigma(E)N_{\text{H}}} \times \left[ A \times E^{-\Gamma} + (\text{Si XIII K}\alpha + \text{Si XIV K}\alpha + \text{Si XIV K}\beta + \text{S XV K}\alpha + \text{S XVI K}\alpha)_{z=z_{\text{red}}} + (\text{Si XIII K}\alpha + \text{Si XIV K}\alpha + \text{Si XIV K}\beta + \text{S XV K}\alpha + \text{S XVI K}\alpha)_{z=z_{\text{blue}}} \right], \quad (2)$$

where the helium-like emission lines include the resonance and forbidden components, and the other annotations of this model are the same as those in § 3.2.1. The emission lines were found to be broad also in this energy band, and the Gaussian width was obtained to be  $\sigma = 5.0^{+1.1}_{-0.9}$  eV, or  $840^{+180}_{-150}$  km s<sup>-1</sup> in terms of the Doppler velocity dispersion.

The most important information obtained from these fits is the relation between the widths of low-energy and high-energy lines. The velocity dispersion of the high energy lines is significantly larger than that of the low-energy lines.

## 4 DISCUSSION AND SUMMARY

### 4.1 Line Fluxes

An intensity ratio of the K $\alpha$  line from Fe XXVI to that of Fe XXV provides a clear temperature indicator for very hot plasmas, and hence can be used to constrain the jet parameters of SS 433. By comparing the ASCA measurements with detailed model calculations, Kotani et al. (1996) estimated the typical initial temperature of the jets to be  $T_0 \sim 20$  keV. In the observation ID-1942, the intensity ratios were obtained as  $0.46 \pm 0.17$  and  $0.42 \pm 0.17$ , for the blue and red jet, respectively, which translate to  $T_0 = 19.5^{+8.8}_{-6.9}$  and  $T_0 = 17.2^{+8.0}_{-6.7}$  keV. From these values, the jet activity of SS 433 is inferred to have been in a normal state during this observation.

In contrast, Marshall et al. (2002) derived significantly lower values based on observation ID-0106. The Fe XXVI lines from the jets were so weak that the intensity ratios of the iron lines were  $0.30 \pm 0.12$  and  $0.17 \pm 0.08$  for the blue and red jets, respectively, yielding  $T_0 = 12.9^{+4.7}_{-4.3}$  and  $T_0 = 8.6^{+2.4}_{-2.1}$  keV. Because these temperatures are lower than the usually reported values, it appears that the high-energy lines, emitted near the base of the jet of SS 433, were at that time hidden by something, such as an expanded accretion disk. Thus, it is likely that SS 433 was in an unusual state during the observation of ID-0106. The same goes for observation ID-1019.  $T_0$  was calculated as  $10.9^{+5.5}_{-4.4}$  keV and  $T_0 = 29.6^{+5.4}_{-10.2}$  keV for the blue and red jet, respectively. Considering SS 433 was in an eclipse at that occasion, the temperature of the blue jet is a reasonable value, while that of the red jet is too high. Such a high temperature of the red jet was often seen during X-ray eclipses (Kotani 1998), but the cause of this phenomenon is yet to be discovered.

### 4.2 Line Widths

The Doppler-shifted lines of SS 433 have been successfully represented by broad Gaussian models. The obtained Doppler velocity dispersion are  $v_{\text{Fe}} = 2100^{+600}_{-340}$  km s<sup>-1</sup> and  $v_{\text{Si}} = 840^{+180}_{-150}$  km s<sup>-1</sup>, for the high-energy (mainly iron) and low-energy (mainly silicon) lines, respectively. Figure 3 summarizes the velocity dispersion of various K $\alpha$  lines, from the present work, as a function of the atomic number. Thus, all measurements agree very well on the low-energy lines, while not on the high-energy lines. This may be caused by the low activity of SS 433 during the observation ID-0106, as suggested by the low  $T_0$ .

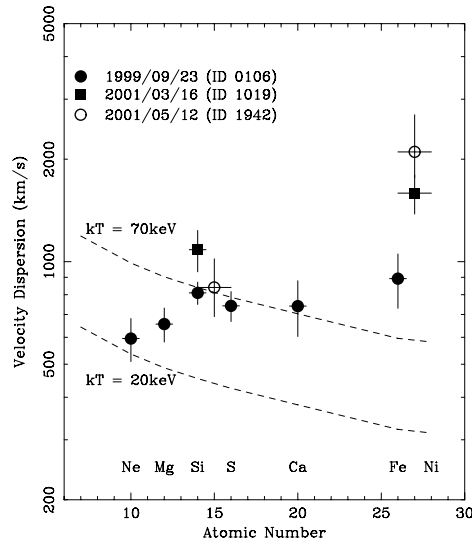


**Fig. 3** Atomic number of  $K\alpha$  line vs. its velocity dispersion. The filled and open circles correspond to the Chandra HETGS observation ID-0106 and -1942, respectively. The filled squares indicate the data obtained on ID-1019. The dashed lines are velocity dispersions of the  $K\alpha$  lines expected for thermal Doppler broadening. The upper one is for an ion kinetic temperature of 70 keV, and lower is for 20 keV.

In figure 3, the dashed curves represent the velocity dispersion expected when the line widths are caused solely by thermal broadening, for two representative ion kinetic temperatures. Thus, the measured line widths are too large to be explained in terms of thermal Doppler effect, for a reasonable range of temperature. Furthermore, the measured positive correlation of the velocity dispersion on the atomic number is opposite to what is predicted by the thermal Doppler effect. For these reasons, the thermal broadening is concluded to be inappropriate as an account of the measured line widths.

The Compton scattering is another candidate of generating the line widths. The X-rays lines may be narrow when produced in the jets, and then Compton scattered in a surrounding medium to get broadened. This may work, if the optical depth of the jets to the electron scattering would be of the order of unity. In this case, a single Compton scattering in a medium of electron temperature  $T_e$  is expected to shift the X-ray energy  $E$  by  $\Delta E \sim E(4kT_e - E)/m_e c^2$ . Then, the measured values of  $\Delta E \sim 5$  eV for silicon ( $E \sim 1.8$  keV) and  $\Delta E \sim 45$  eV for iron ( $E \sim 6.7$  keV) require  $T_e \simeq 0.8$  keV and 2.5 keV, respectively. The discrepant values of  $T_e$  may be explained by a picture that the high-energy lines are produced in a region closer to the central engine. However, such a scattering medium, having the necessary Compton optical depth and the inferred low  $T_e$ , would inevitably produce prominent edges from partially ionized atoms, which are not seen in the spectra. Therefore, Compton scattering may not be appropriate, either.

Another possible origin of the line widths and its dependence on the atomic number is a progressive collimation of the conical opening angle of the jets (figure 4). Marshall et al. (2002) ascribed the line widths to the Doppler broadening that may result from the conical jet outflow, and concluded that the emission occurs in a freely expanding region of constant collimation with an opening half-cone angle of  $\Theta = 1^\circ.23$ ; the opening angle produces a transverse velocity of the jet, which causes the obtained widths. Assuming an oppositely directed pair of jets observed at an angle  $\alpha$  to the line of sight, the Doppler shifts of the blue and red jets are given by  $1 + z =$

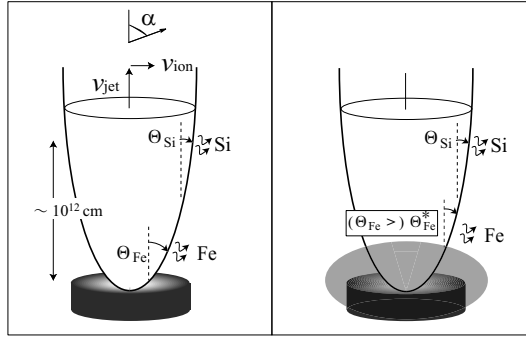


**Fig. 4** A schematic view of a conical jet outflow. The axis of the jet crosses the line of sight at an angle  $\alpha$ . The jet material flows with an opening half-cone angle of  $\Theta_{\text{ion}}$ , which is determined by an axial velocity  $v_{\text{jet}}$  and a transverse velocity  $v_{\text{ion}}$ . The right panel shows the case which the base of the jets was hidden by something (black mesh).

$\gamma \{1 \pm \beta \cos(\alpha)\}$ , where  $\beta$  is the velocity of the jet in unit of  $c$ , and  $\gamma = (1 - \beta^2)^{-1/2}$ . Solving this equation for  $\gamma$  as  $v_{\text{jet}} = \beta \times c = \{1 - (1 + z_{\text{av}})^{-2}\}^{1/2} \times c$ , where  $z_{\text{av}} = (z_{\text{bl}} + z_{\text{rd}})/2$ , and utilizing the observed redshifts,  $v_{\text{jet}} = 0.2629 c$  and  $\alpha = 92^\circ.1$  are obtained.

The velocities of the perpendicular component against the direction of jet traveling are obtained as  $v'_{\text{Fe}} = v_{\text{Fe}} \sin(\alpha) = 2100 \text{ km s}^{-1}$  and  $v'_{\text{Si}} = v_{\text{Si}} \sin(\alpha) = 840 \text{ km s}^{-1}$ . The velocity dispersion can be equated directly with  $f v_{\text{jet}} \tan(\Theta)$ , where  $f$  is a form factor depending on the emissivity distribution across the jet cross section. Assuming that the density is uniform through the cone's cross section and that the component of the velocity which is parallel to the jet axis is the same for all fluid elements in the slice, then a simple calculation gives  $f = 0.74$  (Marshall et al. 2002). Therefore, the present observation yields  $\Theta_{\text{Fe}} = \tan^{-1}(\frac{1}{f} \frac{v'_{\text{Fe}}}{v_{\text{jet}}}) = 2^\circ.1^{+0^\circ.6}_{-0^\circ.3}$ ,  $\Theta_{\text{Si}} = \tan^{-1}(\frac{1}{f} \frac{v'_{\text{Si}}}{v_{\text{jet}}}) = 0^\circ.8 \pm 0^\circ.2$ . The other two data also exhibits finite widths, which correspond to  $0^\circ.9 \pm 0^\circ.2$  and  $0^\circ.8 \pm 0^\circ.1$  (ID-0106), and  $1^\circ.6 \pm 0^\circ.2$  and  $1^\circ.1 \pm 0^\circ.2$  (ID-1019) for the high-energy and low-energy lines, respectively. Since the Fe-K lines are thought to be produced close to the central engine while the Si-K lines to come from those positions of the jets which are  $\geq 10^{12}$  cm away from the center (Kotani 1998), the present results imply that the jet collimation is achieved over a distance of  $\geq 10^{12}$  cm, or  $\geq 10^2$  sec. In the case of ID-0106, the weak Fe lines were obtained, so if the accretion disk is indeed expanded, then the the observed angle would be small as was estimated ( $\Theta_{\text{Fe}}^*$  in the right pannel of figure 4). The similar thing would happen during the eclipse, as seen in ID-1019. While, the opening angles of Si lines, this may not be affected the expanded disk or the X-ray eclipse. Thus, it is consistent with the almost constant values of the angles of the Si lines in these observations.

Since the collimation is thus inferred to occur on a scale much larger than the accretion disk, it is more likely to be achieved by a global mechanism, rather than by any local structure.

## References

- Gladyshev S. A., Goranskii V. P., Cherepashchuk A. M., 1987, *Sov. Astron.*, 31, 541  
 Kotani T., Kawai N., Matsuoka M., Brinkman W., 1996, *PASJ*, 48, 619  
 Kotani T., 1998, PhD Thesis, University of Tokyo  
 Marshall H. L., Canizares C. R., Schulz N. S., 2002, *ApJ*, 564, 941  
 Namiki M., Kawai N., Kotani T., Makishima K., 2003, *PASJ*, 55, 281  
 Namiki M., 2003, PhD Thesis, Tokyo University of Science